Unveiling the Multifunctional Behavior of $NaXTe_2$ (X = Al, Ga, In) Ternary Tellurides: A First-Principles Perspective

M. Elbaa[a,*], S. Haireche[b], A. Khelefhoum[c, d], S. Maabed[d] and M. Bouchenafa[d]

[a] *Laboratory of Energy and Intelligent Systems, Faculty of Matter Sciences and Computer Science, University of Khemis Miliana, 44225, Algeria*
[b] *Laboratory of Mechanics, Physics, and Mathematical Modelling, University of Medea, Medea 26000, Algeria*
[c] *University of Science and Technology Houari Boumediene, Faculty of Electrical Engineering, Automatic Department, BP.32, El-Alia, Bab Ezzouar, 16111 Algiers, Algeria*
[d] *Laboratoire de Matériaux pour Application et Valorisation des Energies Renouvelable (LMAVER), Département de Sciences de la Matière, Université Amar Telidji Laghouat, BP 3000, Algeria*

Received: 23.09.2025 & Accepted: 13.01.2026

Doi: 10.12693/APhysPolA.149.78 *e-mail: m.elbaa@univ-dbkm.dz

This work presents a novel and in-depth first-principles investigation of the ternary telluride compounds $NaXTe_2$ (X = Al, Ga, In) with the aim to systematically uncover their structural, electronic, elastic, and optical characteristics. Using density functional theory calculations, we report for the first time, within a unified framework, a comparative analysis of these compounds crystallizing in the tetragonal $I_{4/mcm}$ space group. Structural optimization yields lattice parameters in excellent agreement with experimental data, confirming the validity of the computational approach. A key finding of this study is the identification of direct band gaps at the Z point for all the investigated compounds, with significantly different values (1.28 eV for $NaAlTe_2$, 0.23 eV for $NaGaTe_2$, and 0.58 eV for $NaInTe_2$), which have not been consistently reported in the literature. The projected density of states reveals pronounced hybridization between the X and Te orbitals, shedding new light on the nature of covalent bonding in the lattice. From a mechanical standpoint, the full elastic tensor, including directional-dependent moduli, demonstrates the mechanical stability and ductility of these compounds, while also quantifying their moderate hardness — a desirable feature for practical integration in devices. Notably, optical analyses reveal a strong absorption in the ultraviolet range, accompanied by favorable dielectric responses and refractive indices, indicating high potential for these materials in ultraviolet-optoelectronic and photovoltaic applications. Overall, this study introduces new insights into the multifunctional behavior of $NaXTe_2$ compounds, establishes a reference dataset for future experimental validation, and highlights these materials as promising candidates for the development of next-generation semiconductors and optical devices.

topics: telluride materials, density functional theory (DFT), condensed matter, band gap

1. Introduction

Ternary chalcogenide materials with the general formula AXQ_2 (where A denotes an alkali or alkaline-earth metal; X represents Al, Ga, or In; and Q stands for S, Se, or Te) belong to a class of crystals that have drawn significant research interest because of their diverse structural chemistry and exceptional physical properties [1–4]. Ternary telluride compounds have attracted considerable interest due to their promising electronic, elastic, and optical properties, making them potential candidates for various technological applications, including thermoelectric materials, optoelectronics, and energy storage devices [5–10]. This includes their use in nonlinear optical devices operating in the near- and mid-infrared wavelength ranges [11]. In addition, these materials could be used in devices such as logic transistors, field effect transistors (FETs), photodetectors, and photoelectrochemical cells [12]. They are also promising for use in optoelectronic device applications because of their various crystalline phases and remarkable properties

associated with thermoelectric effects [13]. Besides that, chalcopyrite semiconductors offer a wide range of optoelectronic applications due to their band gap energies, which cover a broad spectral range from red to ultraviolet light [14–16]. On the other hand, frequency-doubling devices also enable the extension of ranges of powerful lasers (such as CO_2 lasers) from the far-infrared to the mid-infrared region [17]. Furthermore, ternary chalcopyrite compounds show great potential for solar cell applications [18–20].

While most research on AMQ_2 materials has focused on lithium-containing compounds ($LiMQ_2$ materials) [21–25], our study takes a unique approach by exploring the lesser-known sodium chalcogenide materials, specifically $NaXTe_2$ materials. The relative scarcity of research on these materials, possibly due to their growth challenges and air sensitivity, underscores the novelty and importance of our investigation. By focusing on these less-studied materials, we aim to provide a fresh perspective and contribute to the growing body of knowledge in the field of materials science and optoelectronics.

In this study, we investigate the structural, electronic, elastic, and optical properties of $NaXTe_2$ (X = Al, Ga, In) using first-principles calculations based on density functional theory (DFT). This approach allows us to accurately predict and analyze the properties of $NaXTe_2$ compounds, providing valuable insights into their potential applications. We present a comprehensive and in-depth analysis of their structural stability, electronic band structures, density of states, mechanical behavior, and optical response. The findings provide valuable insights into these materials' fundamental characteristics, offering guidance for future experimental and technological advancements.

2. Computational methods and geometric model

Within this research work, a comprehensive investigation of the structural, electronic, elastic, and optical properties of the ternary tellurides $NaXTe_2$ (X = Al, Ga, In) was conducted using first-principles calculations in the framework of density functional theory (DFT) [26]. The computations were performed using the plane-wave pseudopotential (PP-PW) method implemented in the CASTEP code [27]. Ultrasoft pseudopotentials [28] were employed to model electron–ion interactions, particularly in the core regions, while exchange correlation effects were treated using the generalized gradient approximation (GGA) according to the Perdew–Burke–Ernzerhof (PBE) functional [29]. To improve the accuracy of the electronic band gap prediction, the hybrid functional approach (HSE06) was also applied [30]. Structural optimizations were carried out using the

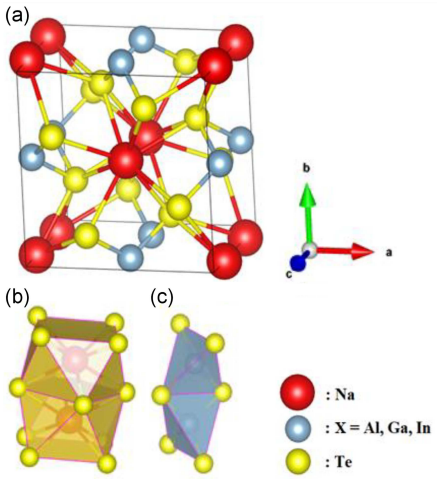

Fig. 1. Schematic illustration of (a) the conventional tetragonal unit cell of $NaXTe_2$ (X = In, Ga, Al), (b) two $NaTe_8$ octahedral and (c) two XTe_4 tetrahedral unit sites.

Broyden–Fletcher–Goldfarb–Shanno (BFGS) minimization algorithm [31], which allows for simultaneous relaxation of lattice parameters and atomic positions to obtain the ground-state configuration. The choice of pseudopotentials enabled accurate representation of the valence electron configurations: Na ($2s^2 2p^6 3s^1$), Al ($3s^2 3p^1$), Ga ($3d^{10} 4s^2 4p^1$), In ($4d^{10} 5s^2 5p^1$), and Te ($5s^2 5p^4$). Self-consistent field (SCF) calculations were considered with the following stringent criteria: total energy variation below 10^{-6} eV/atom, maximum Hellmann–Feynman ionic force below 0.005 eV/Å, maximum atomic displacement below 10^{-4} Å, and maximum stress component under 0.01 GPa. For the plane-wave basis set, akinetic energy cut-off of 700 eV was adopted, which ensured reliable convergence. The Brillouin zone was sampled using a Monkhorst–Pack grid of $6 \times 6 \times 5$ k-points, which provided satisfactory convergence for all calculated properties. All compounds were structurally optimized at zero temperature and zero external pressure and were found to crystallize in a body-centered tetragonal lattice with space group $I_{4/mcm}$ (no. 140), characterized by lattice constants $a = b \neq c$ and angles $\alpha = \beta = \gamma = 90°$ [5, 6, 32]. The equilibrium structures, visualized using the VESTA software [33], are presented in Fig. 1.

A conventional cell has a total of 4 atoms: two telluride atoms (Te) occupying the 8h positions of $NaXTe_2$, one (Na) atom located in the 4a position $(0, 0, 0.25)$, and one X atom (where X = Al, Ga, In) located at the 4b position $(0, 0.5, 0.25)$. In this tetrahedral phase, the Na atoms are situated in an octahedral environment surrounded by 8 telluride (Te) atoms in a non-congestive $NaTe_8$ manner. In contrast, each cation X atom is tetrahedrally coordinated by four Te nearest neighbors, forming XTe4 units.

TABLE I

Lattice parameters and cell volume of the ternary $NaXTe_2$ compounds (X = Al, Ga, and In) compared with other experimental and theoretical data, including the relative deviations (d) and compounds density (ρ)

Compound	Method type	a [Å]	b [Å]	c [Å]	V [Å^3]	ρ [g/cm^3]	Ref.
$NaAlTe_2$	cal.	8.3091	8.3091	6.8835	475.244	–	our result
	exper.	8.310	8.310	6.710	463.366	4.37	[5]
	other	8.239	8.239	6.887	467.497	4.34	[34]
	d [%]	0.01	0.01	2.57	2.56	–	–
$NaGaTe_2$	cal.	8.298	8.298	6.893	474.579	–	our result
	exper.	8.220	8.220	6.880	464.870	4.97	[6]
	other	8.204	8.204	6.876	462.793	4.99	[35]
	d [%]	0.93	0.93	0.18	2.08	–	–
$NaInTe_2$	cal.	8.415	8.415	7.282	515.707	–	our result
	exper.	8.330	8.330	.270	504.5	5.16	[36]
	other	8.39	8.39	7.272	511.9	5.17	[32]
	d [%]	1.02	1.02	0.16	2.22	–	–

TABLE II

Atomic positions of the ternary $NaXTe_2$ compounds (X = Al, Ga, and In). Here, W.P. means Wyckoff positions.

Compound	Atom	W.P.	x		y		z	
			Exper.	Cal.	Exper.	Cal.	Exper.	Cal.
$NaAlTe_2$	Na	4a	0.0000	0.00000	0.0000	0.00000	0.2500	0.2500
	Al	4b	0.0000	0.00000	0.5000	0.50000	0.2500	0.2500
	Te	8h	0.1691	0.17344	0.6691	0.67344	0.0000	0.0000
$NaGaTe_2$	Na	4a	0.0000	0.00000	0.0000	0.00000	0.2500	0.2500
	Ga	4b	0.0000	0.00000	0.5000	0.50000	0.2500	0.2500
	Te	8h	0.1734	0.17525	0.6734	0.67525	0.0000	0.0000
$NaInTe_2$	Na	4a	0.0000	0.00000	0.0000	0.0000	0.2500	0.2500
	In	4b	0.0000	0.00000	0.5000	0.5000	0.2500	0.2500
	Te	8h	0.1800	0.18577	0.6800	0.68577	0.0000	0.0000

3. Results and discussion

3.1. Structural properties

The $NaXTe_2$ compounds crystallize in a tetragonal structure belonging to the space group $I_{4/mcm}$ (no. 140), characterized by specific atomic arrangements that influence their physical properties. In this work, the lattice parameters a and c of the ternary compounds $NaXTe_2$ (X = Al, Ga, In) were computed at zero pressure using structural optimization. The optimized values are presented in Table I, together with previously reported theoretical results for comparison [5, 6, 32, 34–36]. Furthermore, Table I offers a direct comparison between the calculated lattice parameters and available experimental data for the three compounds. According to the density functional theory (DFT) reliability criteria proposed by T. Helaimia [5], the obtained results exhibit excellent agreement with both experimental and theoretical benchmarks. Quantitatively, the relative deviations between our computed values and experimental measurements are remarkably low: for $NaAlTe_2$ the relative errors are 0.01% and 2.57% for a and c, respectively; for $NaGaTe_2$, they are 0.93% and 0.18%; and for $NaInTe_2$ — 0.02% and 0.16%. The corresponding relative volume errors are 2.56%, 2.08%, and 2.22% for $NaAlTe_2$, $NaGaTe_2$, and $NaInTe_2$, respectively, confirming the reliability of the structural optimization process. The observed trend in unit cell volume, i.e., $V_{NaInTe_2} > V_{NaAlTe_2} > V_{NaGaTe_2}$, can be attributed to the progressive increase in the atomic radius of the cation X, with values $R_{Al} = 1.18$ Å, $R_{Ga} = 1.36$ Å, and $R_{In} = 1.44$ Å. This confirms that

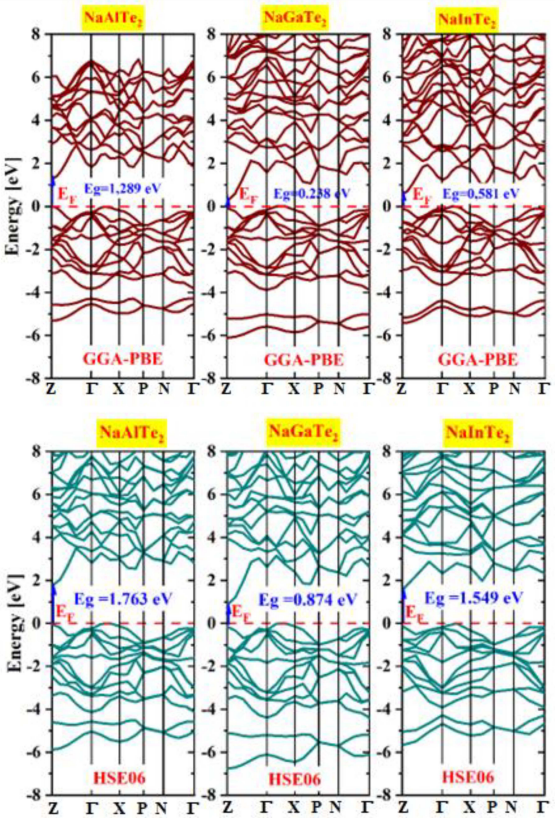

Fig. 2. Calculated electronic band structures of $NaXTe_2$ compounds (X = Al, Ga, In) at their ground-state lattice constants along the high-symmetry paths of the Brillouin zone. The compounds' electronic band structures were calculated using the GGA-PBE and HSE06 methods. The position of the Fermi level is shown by a dashed horizontal red line.

the lattice expansion correlates with the increasing size of the substituting cation, as expected from crystallographic considerations.

The atomic positions of Na, Al, Ga, and In exhibit no variation (with negligible relative errors), indicating stable and well-converged configurations. In contrast, slight deviations are observed in the positions of Te atoms along the Cartesian axes. Specifically, the Te atoms show relative shifts along the x axis of 2.57%, 1.07%, and 3.21% for $NaAlTe_2$, $NaGaTe_2$, and $NaInTe_2$, respectively, and along the y axis of 0.65%, 0.27%, and 0.85% for the same compounds. Notably, the positions of Te atoms along the z axis remain unchanged in all three compositions. These variations are within acceptable limits and are likely attributed to relaxation effects during structural optimization. Overall, the computed atomic positions are in good agreement with the experimental data (see Table II), further validating the reliability of the theoretical approach.

Table III reports the calculated interatomic distances for the three $NaXTe_2$ compounds (X = Al, Ga, In), together with available experimental

TABLE III

Interatomic distances Na–Te and X–Te of the ternary $NaXTe_2$ compounds (X = Al, Ga, and In).

Compound	Band	Interatomic distances [Å]		
		Cal.	Exper. [Ref.]	Other [Ref.]
$NaAlTe_2$	Na–Te	3.52	3.52 [37]	3.51 [5]
	Al–Te	2.66	2.67 [38]	2.60 [5]
$NaGaTe_2$	Na–Te	3.51	3.4–3.6 [38]	3.49 [6]
	Ga–Te	2.68	2.63 [39]	2.65 [6]
$NaInTe_2$	Na–Te	3.57	3.56 [38]	3.56 [32]
	In–Te	2.86	2.83 [39]	2.79 [32]

data [37, 38] and previous theoretical studies [5, 6, 32]. In the crystal structure of these materials, each sodium (Na) atom is coordinated by eight tellurium (Te) atoms, forming a distorted square antiprism configuration, denoted as $NaTe_8$. The calculated Na–Te bond lengths are 3.52 Å for $NaAlTe_2$, 3.49 Å for $NaGaTe_2$, and 3.56 Å for $NaInTe_2$. Additionally, the cationic X atoms (Al, Ga and In) are each surrounded by four Te atoms in a slightly distorted tetrahedral geometry (XTe_4). The corresponding X–Te bond lengths were found to be 2.60 Å for $NaAlTe_2$, 2.65 Å for $NaGaTe_2$, and 2.79 Å for $NaInTe_2$. These interatomic distances show very good agreement with experimental measurements, confirming the accuracy and reliability of the structural predictions obtained through first-principles calculations.

3.2. Electronic properties

3.2.1. Band structure

In this study, the electronic band structures of $NaXTe_2$ compounds (X = Al, Ga and In) were computed at specific high-symmetry points Z $(-\frac{1}{2}, 0, \frac{1}{2})$, Γ $(0, 0, 0)$, X $(0, 0, \frac{1}{2})$, P $(\frac{1}{2}, \frac{1}{2}, \frac{1}{2})$, and N $(0, \frac{1}{2}, 0)$ within the first Brillouin zone, following full structural optimization, as illustrated in Fig. 2. The results reveal that both the valence band maximum (VBM) and the conduction band minimum (CBM) are located at the Z point for all three compounds. This configuration confirms that $NaAlTe_2$, $NaGaTe_2$, and $NaInTe_2$ are direct band gap semiconductors, with calculated band gap energies of 1.28, 0.23, and 0.58 eV, respectively. For details, see Table IV [5, 6, 32, 39]. A notable trend is observed in the variation of band gap energies, namely the gap decreases systematically from $NaAlTe_2$ to $NaInTe_2$. For instance, the energy gap reduces from 1.763 eV for $NaAlTe_2$ to 0.87 eV for $NaGaTe_2$, suggesting that the atomic number of the cation (X) significantly influences the electronic properties

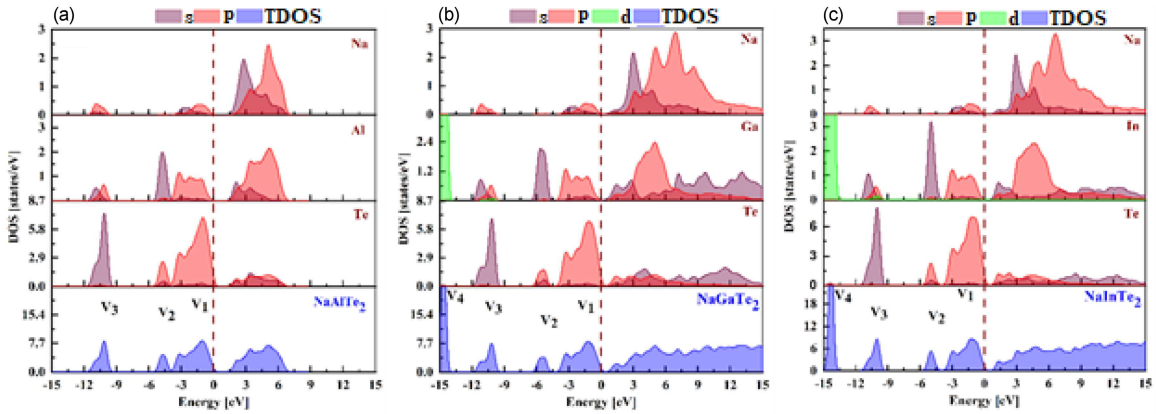

Fig. 3. Calculated total densities of states (TDOS) and atom-resolved, angular momentum-projected partial densities of states (PDOS) for (a) $NaAlTe_2$, (b) $NaGaTe_2$ and (c) $NaInTe_2$.

of these compounds. The reduction indicates that heavier cations contribute to band gap narrowing, likely due to enhanced relativistic effects and stronger orbital hybridization. Furthermore, the choice of the exchange–correlation functional in the DFT framework plays a pivotal role in the accuracy of band gap predictions. The HSE06 hybrid functional provides values that are in better agreement with experimental observations than those obtained using the conventional GGA-PBE method. Additionally, other extrinsic physical factors, such as oxygen vacancies reported by Haireche [40] or applied pressure studied by Kermezli [41], can further influence and reduce the optical band gap, highlighting the complex interplay between intrinsic material properties and external conditions.

3.2.2. Density of states (DOS)

Figure 3 illustrates the total and partial density of states (DOS) for $NaAlTe_2$, NaGaTe and NaInTe, highlighting the distinct electronic structures of these compounds. This study provides a deeper understanding of these three compounds. The valence band consists of four main regions: V1, V2, V3, and V4, though the V4 band region is absent in $NaAlTe_2$.

- The V1 region is primarily formed by inter-*p*-orbital hybridization of Na, X, and Te atoms, indicating the presence of covalent bonding between X and Te in all three compounds.
- The V2 region results from the combination of the *s* and *p* orbitals of X and Te atoms, further confirming the interaction between these elements.
- The V3 region originates mainly from the hybridization of the *s* orbitals of X and Te, with a major contribution from Te, along with the *p* orbitals of Na and X.

TABLE IV

Calculated band gaps for $NaXTe_2$ compounds (X = Al, Ga, In) and their corresponding experimental and theoretical data for some isostructural compounds using the GGA-PBE and HSE06 methods.

E_g [eV]	Gap energy	Transition	Method	Ref.
$NaAlTe_2$				
1.289	direct	Z–Z	GGA	our work
1.763	direct	Z–Z	HSE06	our work
1.233	direct	Z–Z	GGA	[5]
1.641	direct	Z–Z	HSE06	[5]
$NaGaTe_2$				
0.238	direct	Z–Z	GGA	our work
0.87	direct	Z–Z	HSE06	our work
1.2	direct	–	mBJ	[6]
$NaInTe_2$				
0.581	direct	Z–Z	GGA	our work
1.54	direct	Z–Z	HSE06	our work
1.8	direct	Z–Z	HSE06	[32]
1.6	direct	–		[39]

- The V4 region, present only in $NaGaTe_2$ and $NaInTe_2$, is primarily associated with the *d* orbitals of X, which are absent in the element Al.

The conduction bands are positioned close to the Fermi level and emerge from the combination of the *s* and *p* orbitals of all constituent elements in each compound. This distribution of electronic states indicates that the electronic properties of $NaXTe_2$ materials are highly dependent on atomic hybridization, exhibiting notable variations depending on the selected X element (Al, Ga, or In). A comparable phenomenon was reported by Haireche et al. [42] for SrX systems, where X corresponds to Se or Te,

TABLE V

Results of the Mulliken population analysis for the investigated ternary compounds.

Compound	Atoms	s	p	d	Total	Charge	Bond population
$NaAlTe_2$	Na	2.26	6.51		8.78	0.22	−0.02 for Na–Te
	Al	1.21	1.72		2.93	0.07	0.23 for Al–Te
	Te	1.63	4.52		6.15	−0.15	–
$NaGaTe_2$	Na	2.29	6.53		8.82	0.18	0.07 for Na–Te
	Ga	1.46	1.76	10.00	13.22	−0.22	−0.31 for Ga–Te
	Te	1.60	4.39		5.98	0.02	–
$NaInTe_2$	Na	2.27	6.50		8.78	0.22	−0.02 for Na–Te
	In	1.60	1.69	9.99	13.28	−0.28	0.01 for In–Te
	Te	1.50	4.47		5.97	0.03	

further underscoring the recurring nature of this effect across different compound configurations, see also [43]. The absence of the V4 region in $NaAlTe_2$ may indicate differences in electronic structure and bonding characteristics compared to $NaGaTe_2$ and $NaInTe_2$.

Table V presents the Mulliken population analysis of three ternary telluride compounds: $NaAlTe_2$, $NaGaTe_2$, and $NaInTe_2$. The analysis includes the s, p, and d orbital contributions, total population, and charge distribution for each atom in the corresponding compounds. The s-orbital populations for Na, Al, Ga, In, and Te remain relatively consistent across the compounds, with Na having the highest s-orbital occupancy ($\sim$ 2.26–2.29). The chalcogen atoms (i.e., telurium) exhibit s-orbital populations in the range of 1.50–1.63, indicating a slight variation with different cation substitutions. Tellurium (Te) has a high p-orbital population ($\sim$ 4.39–4.52), confirming its strong contribution in bonding. The p-orbital contributions of Al, Ga, and In are relatively low (1.69–1.76), suggesting they play a less dominant role in covalent bonding than Te. Notably, Al has no d-orbital population, whereas Ga and In exhibit significant d-orbital contributions ($\sim$ 10.00 and $\sim$ 9.99, respectively). This indicates that Ga and In utilize d orbitals in bonding, possibly contributing to higher hybridization effects and stronger interactions with Te. Sodium (Na) maintains a positive charge (0.18–0.22), indicating its role as a donor (cation). In the $NaXTe_2$ compounds, the B-site elements, i.e., Al, Ga, and In, exhibit distinct charge characteristics that reflect their varying electron-attractive tendencies. Aluminum in $NaAlTe_2$ shows a slightly positive charge of +0.07, indicating a relatively weak electron affinity. In contrast, gallium in $NaGaTe_2$ carries a negative charge of −0.22, revealing a stronger tendency to gain electrons compared to Al. Indium in $NaInTe_2$ exhibits an even more negative charge of −0.28, suggesting the highest electron affinity among the three elements. Meanwhile, tellurium (Te) maintains nearly neutral to slightly negative charge values, ranging from −0.15 to 0.03 in all compounds, thereby confirming its consistent role in facilitating redistribution of electron density within the crystal structure. The Na–Te bond population remains similar in all compounds (−0.02 to 0.07), suggesting that the alkali metal's interaction with Te is weakly ionic. The Ga–Te bond (−0.31) in $NaGaTe_2$ shows a more negative population, indicating a stronger interaction than the Al–Te and In–Te bonds. The Al–Te and In–Te bond populations are relatively small (0.23 and 0.01, respectively), suggesting a weaker covalent character compared to the Ga–Te bond. $NaGaTe_2$ and $NaInTe_2$ exhibit stronger covalent interactions due to significant d-orbital participation. $NaAlTe_2$ appears to be the most ionic, as Al lacks d-orbital contributions. Ga shows the strongest interaction with Te, likely due to its higher electronegativity and d-orbital participation. $NaGaTe_2$ emerges as the most covalent compound, with higher d-orbital participation and a stronger Ga–Te bond. $NaAlTe_2$ shows the weakest covalent interactions, making it the most ionic in nature. $NaInTe_2$ display characteristics similar to $NaGaTe_2$, but with a slightly weaker bond strength.

3.3. Elastic properties

3.3.1. Elastics constants

Elastic constants of a material provide crucial information about the types of forces operating within it, as well as the connection between its mechanical and dynamic properties. Specifically, they offer insights into the stability and rigidity of materials [44, 45]. In Voigt's notation, $NaXTe_2$ (X =Al, Ga, In) compounds exhibit a tetragonal crystal structure, and their elasticity tensor consist of six independent components: C_{11}, C_{33}, C_{44}, C_{66}, C_{12} and C_{13} [44, 45].

These constants represent different components of the stiffness tensor, which describe how the material deforms under various stress conditions. Specifically, C_{11} quantifies the stiffness in the direction

TABLE VI

Elastic constants C_{ij} [in GPa] of the ternary compounds $NaXTe_2$ (X = Al, Ga, and In).

Compound	C_{11}	C_{33}	C_{44}	C_{66}	C_{12}	C_{13}	Ref.
$NaAlTe_2$	47.70	71.85	28.16	13.18	33.39	23.90	our work
	41.30	84.25	15.73	16.18	28.12	17.41	[48]
$NaGaTe_2$	34.84	71.15	10.39	13.50	22.69	11.48	our work
	70-90	80-100	15-25	20-30	20-30	25–35	[48]
$NaInTe_2$	46.91	67.42	23.73	12.82	28.16	21.92	our work

TABLE VII

Bulk modulus, shear modulus, microhardness, Young's modulus, Poisson's ratio, Debye temperature, universal elastic, anisotropy index (A^U), and average acoustic velocity (v_m) of the ternary compounds $NaXTe_2$ (X = Al, Ga and In) calculated by the GGA method. The subscript 'V', 'R' or 'H' denotes that the modulus was obtained using the Voigt, Reuss, or Hill theory.

Compound	B_V [GPa]	B_R [GPa]	B_H [GPa]	G_V [GPa]	G_R [GPa]	G_H [GPa]	E_H [GPa]	ν_H	B_H/G_H	T_D [K]	A^U	v_m [m/s]
$NaAlTe_2$	36.62	36.25	36.44	19.63	14.99	17.31	44.83	0.15	2.10	249.33	1.56	2170.27
$NaGaTe_2$	25.79	24.88	25.34	13.20	10.60	11.90	30.86	0.15	2.12	234.98	1.26	1688.13
$NaInTe_2$	33.91	33.54	33.73	18.00	15.69	16.85	43.36	0.14	2.00	161.28	0.74	1964.46

parallel to the crystallographic a axis, indicating the material's resistance to deformation along this axis. The components C_{12} and C_{13} describe the interactions between perpendicular stress and strain components, providing insight into how the material reacts when stress is applied in one direction but strain occurs in another [46]. The component C_{33} represents the stiffness along the crystallographic c axis, which is particularly relevant for tetragonal materials like $NaXTe_2$, as they have distinct properties along this axis. Finally, the shear modulus, C_{66}, describes the material's resistance to shear deformation, which is crucial for understanding how the material behaves under forces that cause sliding or twisting.

To assess the mechanical properties of the ternary $NaXTe_2$ compounds, elastic constants and elasticity coefficients were calculated using the GGA-PBE method and the stress–strain approach [47]. The calculated values of these constants are presented in Table VI [48]. The studied materials are mechanically stable according to the Born criteria for mechanical stability in the tetragonal phase [44]. The elastic constants' values are of the same order as the theoretical values reported in [5]. Comparison of C_{ij} calculated for $NaXTe_2$ shows a systematic decrease in these constants as X varies in the order Al $\rightarrow$ In $\rightarrow$ Ga; this indicates that $NaAlTe_2$ is less resistant to shear deformation (under applied stress) than the other two compounds. It is also noted that these compounds are less resistant to shear than to pressure. It is noted that the elastic constant C_{33} is smaller than the elastic constant C_{11}, which indicates that all compounds are stiffer in the [100] and [010] directions than along the [001] direction. Moreover, C_{11} and C_{33} are larger than C_{44} and C_{66}, indicating that these compounds exhibit greater resistance to compressive stress than to shear stress.

Table VII shows the elastic modulus values of our ternary compounds ($NaXTe_2$) in the tetragonal phase of the space group $I_{4/mcm}$ (no. 140), calculated using the GGA-PBE method. Low values of bulk modulus (B) and shear modulus (G) indicate that all compounds show low wear and pressure resistance. This is often an indication of low stiffness. The Voigt–Reuss–Hill (VRH) approximation [5, 49, 50] is used to estimate the compressive moduli B and G.

The Young's modulus (E) indicates whether a material behaves as stiff or soft in its elastic response; a larger value corresponds to a stiffer material. From the obtained results, it appears that the investigated compounds have a small Young's modulus. This means that they behave as soft materials. It is noted that the Young's moduli of the two compounds, $NaAlTe_2$ and $NaInTe_2$, are very close to each other and higher than that of $NaGaTe_2$. Now, Poisson's ratio ν indicates the type of bond between adjacent atomic levels; for covalent compounds, the value is $\nu \simeq 0.1$, while for ionic compounds, the value is $\nu \approx 0.25$ [51, 52]. The ternary compounds $NaAlTe_2$, $NaGaTe_2$ and $NaInTe_2$ have Poisson's ratios of 0.15, 0.15, and 0.14, respectively, which indicates the presence of covalent bonding. The material can also be classified as ductile or brittle by evaluating Poisson's ratio ν, using the Frantsevich criterion applied by Kanchana et al. [53]. According to this criterion, lower values of ν ($< 1/3$) indicate brittleness, whereas higher values ν ($> 1/3$) indicate ductility. Therefore, for our studied compounds with the ν values below 0.33, the Frantsevich criterion

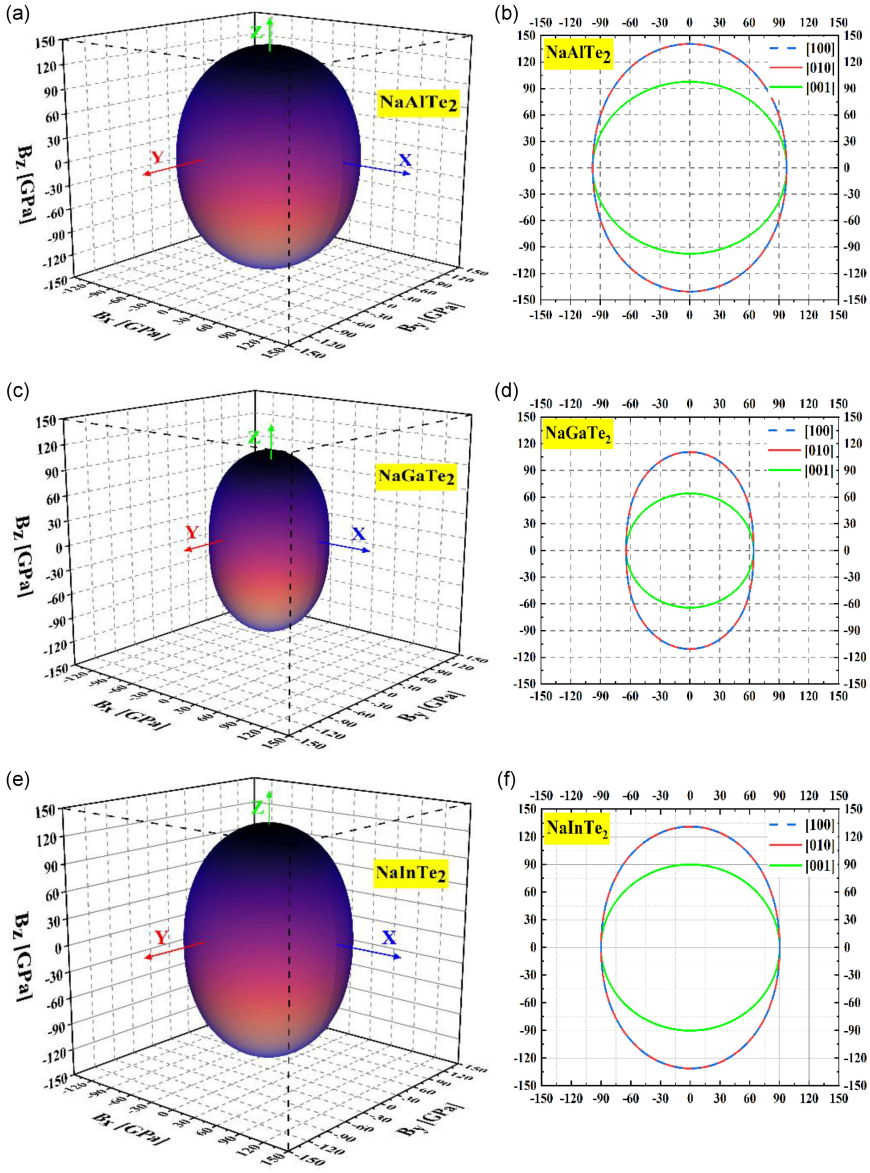

Fig. 4. 3D-representation of the directional dependence of the compressibility coefficient for $NaXTe_2$ (X = Al, Ga, In) (a, c, e) and their cross-sections in selected reticular planes (b, d, f).

actually suggests that the compounds $NaAlTe_2$, $NaGaTe_2$ and $NaInTe_2$ are brittle, not ductile. The B/G ratio also gives an idea of the ductility and brittleness of the material according to the Pugh criterion [54]. According to Pugh, a material is considered ductile if the ratio of bulk modulus to shear modulus, B/G, exceeds 1.75; otherwise, it is classified as brittle (i.e., brittle for $B/G < 1.75$ and ductile for $B/G > 1.75$). For the $NaAlTe_2$, $NaGaTe_2$, and $NaInTe_2$ compounds, the B/G values are 2.10, 2.12, and 2.00, respectively; therefore, these materials are ductile. The degree of elastic anisotropy can be estimated using the universal anisotropy index A^U as defined in [55]. A crystal is isotropic when $A^U = 0$; otherwise, it is anisotropic. The elastic properties of all known crystals are anisotropic [5, 56]. The Debye temperatures were calculated at zero temperature and low pressure. Experimental data on the elastic properties of these compounds are currently unavailable.

3.3.2. Representation of the compounds' anisotropy

Visualizing the directional dependence of the bulk modulus (B) and Young's modulus (E) serves as an effective approach to quantifying elastic anisotropy in materials. Figures 4 and 5 display three-dimensional plots illustrating the variation of B and E along crystallographic directions, together with their two-dimensional cross-sections in the (ab), (ac), and (bc) planes for the $NaXTe_2$ compounds (X = Al, Ga, In).

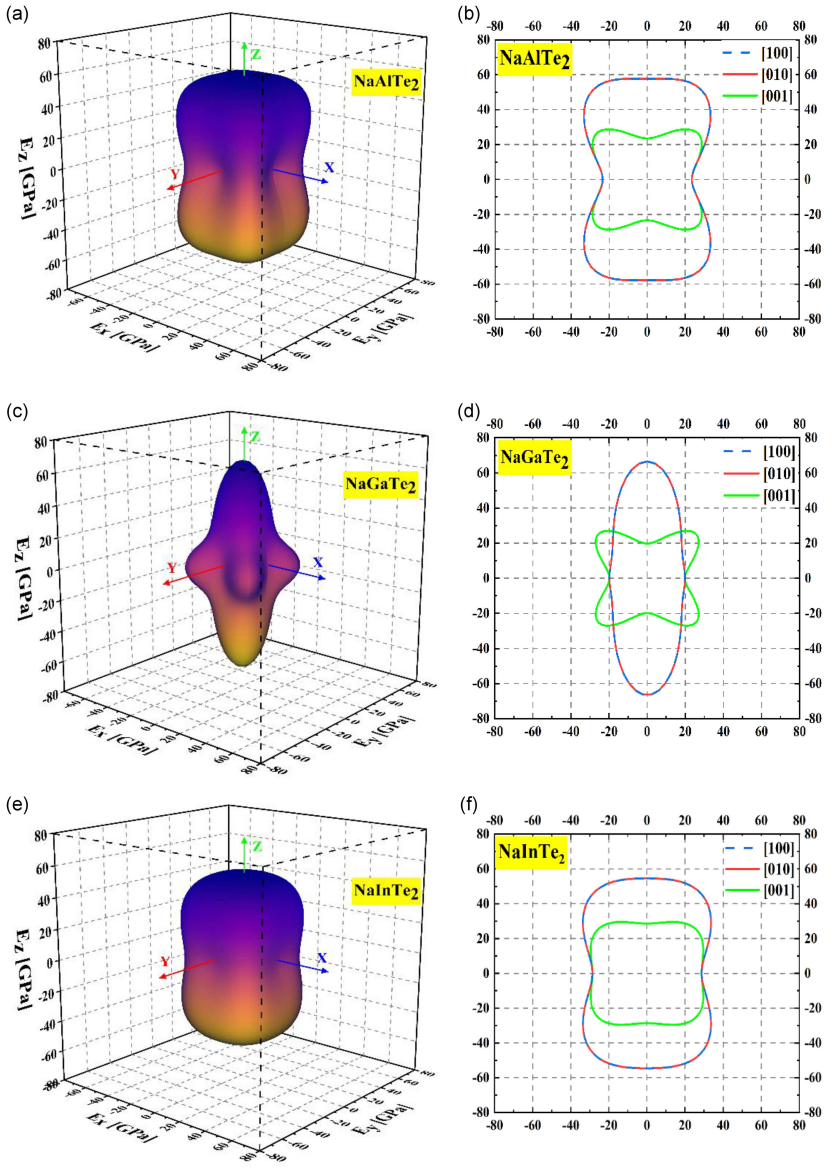

Fig. 5. 3D-representation of the directional dependence of the Young's modulus for $NaXTe_2$ (X= Al, Ga, In) (a, c, e) and their cross-sections in selected reticular planes (b, d, f).

Figure 4 shows a similarity of the anisotropy of the compressibility module B in the direction [001] for the three compounds $NaAlTe_2$, $NaGaTe_2$ and $NaInTe_2$. Giri et al. [57] observed a similar behavior in their experimental study on the $CuInS_2$ compound. Since the compression anisotropy is relatively low in both materials studied, this result can be confirmed by tracing the projections of the compressibility module B in the different planes. This figure shows that the compressibility modulus B along the c-axis for both planes (ac) and (bc) is larger, with values of 140 GPa for $NaAlTe_2$, 110 GPa for $NaGaTe_2$, and 130 GPa for $NaInTe_2$. This indicates that compression along the c-axis is more difficult than along the a and b axes, which have minimum values of 100, 68, and 90 GPa for $NaAlTe_2$, $NaGaTe_2$, and $NaInTe_2$, respectively. It is also noted that the degree of anisotropy in $NaAlTe_2$ and $NaInTe_2$ is higher than in $NaGaTe_2$, especially in the (ac) and (bc) planes. The shape of the compressibility module B in the plane (ab) is circular. This indicates isotropic behavior for the three compounds. The behavior was theoretically modeled by Kossa et al. [58] in the context of isotopic systems.

Figure 5 present the 3D representation of the Young's modulus, showing that the three compounds have anisotropic Young's modulus (E) behavior. This anisotropy was confirmed in Zhang's study [59] on the behavior of quartz under uniaxial compression (see also [60]). The E surfaces of these three compounds deviate from an ideal spherical shape, further indicating their anisotropic response. Similar observations were reported by Challis et al. [61] in their study of the $Ti_{24}Nb_4Zr_8Sn$ alloy. To

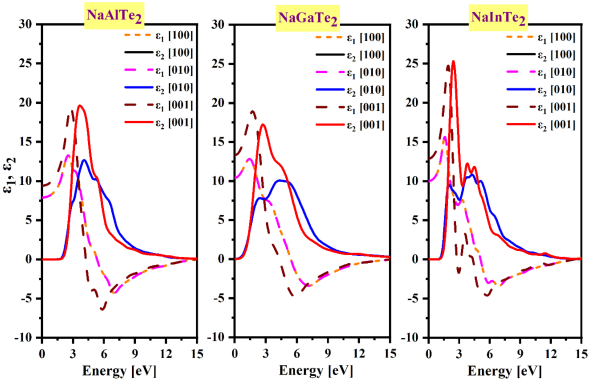

Fig. 6. Dielectric function spectra of ternary chalcogenide compounds $NaXTe_2$ (X = Al, Ga, In).

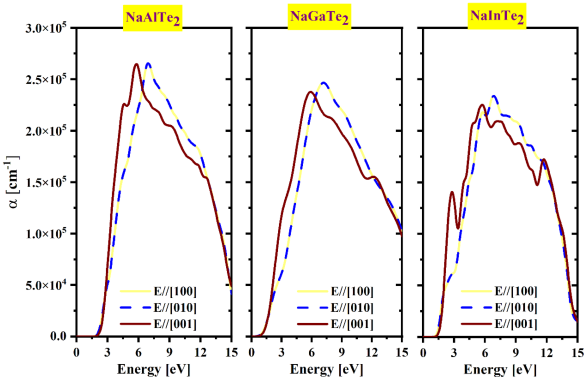

Fig. 7. Absorption spectra of chalcogen ternary compounds $NaXTe_2$.

better describe the anisotropy of the Young's modulus, we trace the intersections of the 3D surfaces with different planes. The extreme values of Young's modulus for the three studied compounds would occur in the (*ac*) and (*bc*) planes when the stress is applied in one of the main directions [100], [010] and [001], where E is 59, 75, and 47 GPa for the compound $NaAlTe_2$, $NaGaTe_2$ and $NaInTe_2$, respectively. On the other hand, the minimum value in the *ab* plane is $E =$ 30 GPa when the stress is applied along the principal crystallographic directions [100] and [010] for all three compounds. Our results of the elastic response to uniaxial traction/compression are identical in both planes (*ac*) and (*bc*). These results support the calculated values of the universal anisotropy index (A^U) for all three compounds.

3.4. Optical properties

3.4.1. Dielectric functions $\varepsilon_1(\omega)$ and $\varepsilon_2(\omega)$

Optical properties of $NaXTe_2$ were calculated under photon illumination up to 15 eV using the GGA approximation. Figure 6 shows the dielectric function at zero pressure; this function is important in solid-state physics within the 0–15 eV energy range. The real part of the dielectric function, $\varepsilon_1(0)$, obtained at the lower end of this energy range for $NaAlTe_2$, $NaGaTe_2$, and $NaInTe_2$ is as follows: 7.89, 10.43, and 10.02 in the [100] direction, respectively, and 9.41, 13.29, and 12.87 in the [001] direction, respectively. The highest peaks of the real part of the dielectric function $\varepsilon_1(\omega)$ calculated for $NaAlTe_2$, $NaGaTe_2$, and $NaInTe_2$ are as follows: 13.28 (2.54 eV), 12.82 (1.41 eV) and 15.62 (1.57 eV) in the [100] direction, respectively, and 19.41 (2.76 eV), 18.92 (1.73 eV) and 24.73 (1.89 eV) in the [001], respectively. Although the magnitude of $\varepsilon_1(\omega)$ changed when the cation is varied from Al $\rightarrow$ Ga $\rightarrow$ In, the overall shape of the function remains unchanged. The largest value of a peak was observed in the compound $NaInTe_2$, followed by $NaAlTe_2$ and $NaGaTe_2$; this order may be due to an interband transition. Each peak of the imaginary part of the dielectric function, $\varepsilon_2(\omega)$, corresponds to an electronic transition, as the imaginary part is associated with the band structure. The calculated amplitude (with corresponding photon energy) of the main peaks for the compounds $NaAlTe_2$, $NaGaTe_2$ and $NaInTe_2$ are 12.67 (4.08 eV), 10.06 (4.33 eV), 10.82 (1.73 eV), respectively, where the light is polarized in the [100] direction, and 19.62 (3.66 eV), 17.23 (2.71 eV), 25.29 (2.41 eV), respectively, where the light is polarized along the [001] direction.

3.4.2. Optical absorption coefficient

Figure 7 shows the calculated absorption (α) spectra of $NaAlTe_2$, $NaGaTe_2$ and $NaInTe_2$ along the (100), (010) and (001) directions in the tetragonal structure. The absorption edge is about 1.93, 0.81, and 1.29 eV, corresponding to the energy difference between the bottom of the valence band and the top of the conduction band at the Z point. The absorption coefficient α increases to approximately 2.65×10^5, 2.46×10^5, and 2.33×10^5 cm^{-1}, corresponding to energies of 6.93, 7.18, and 6.86 eV, where the light is polarized in the [100] direction. In the case where the light is polarized in the [001] direction, the values of α are 2.64×10^5, 2.37×10^5, and 2.52×10^5 cm^{-1}, corresponding to energies of 5.81, 5.88, and 5.74 eV for $NaAlTe_2$, $NaGaTe_2$, and $NaInTe_2$, respectively. The absorption coefficient α decreases progressively when the cation is substituted from Al to Ga and then to In. All three considered compounds exhibit relatively high absorption in the visible range compared to the infrared, but much lower absorption than in the ultraviolet (UV) range. The same remark was indicated in the study by S. Eisebitt et al. [62].

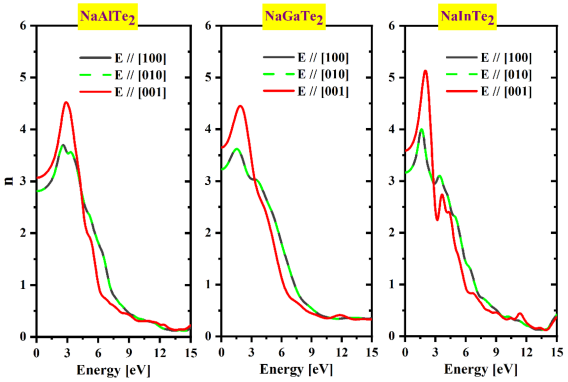

Fig. 8. Refractive index spectra of ternary chalcogen compounds $NaXTe_2$.

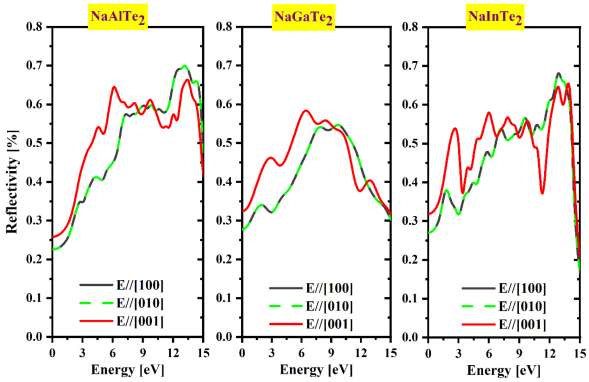

Fig. 9. Reflectivity spectra of ternary chalcogenide compounds $NaXTe_2$.

Other binary semiconductor materials, such as SrX (X = Se, Te, S), exhibit similar behavior under near-UV radiation, highlighting their potential for application in the photovoltaic field [63, 64].

3.4.3. Refractive index

Figure 8 shows the refractive index (n) spectra and extinction coefficient of the $NaXTe_2$ compounds. The static refractive index values $n(\omega = 0)$ are 2.80, 3.23, and 3.16 in the [100] polarization direction. In the [001] direction, the values are 3.06, 3.65, and 3.58 for $NaAlTe_2$, $NaGaTe_2$, and $NaInTe_2$, respectively. The refractive index increases with energy, reaching its maximum value of 2.70 (3.22 eV), 2.60 (3.10 eV), and 2.55 (3.03 eV) in the [100] polarization direction, and 3.54 (3.79 eV), 3.38 (3.84 eV), and 3.36 (3.86 eV) in the [001] polarization direction for the three materials studied ($NaXTe_2$; X = Al, Ga, In). It then decreases to a minimum value of about 0.27. The decrease in n is of particular interest in radiation detection, especially when accompanied by a reduction in reflectivity. This behavior plays a crucial role in enhancing solar radiation transmission, making it highly beneficial for photovoltaic applications [42, 43].

3.4.4. Reflectivity

Figure 9 represents the spectra of reflectivity $R(\omega)$. The maximum values are approximately 69% (13.13 eV), 54% (9.68 eV), and 68% (12.88 eV) in the [100] direction, as well as 66% (13.41 eV), 58% (6.44 eV), and 65% (13.84 eV) in the [001] direction for $NaAlTe_2$, $NaGaTe_2$ and $NaInTe_2$, respectively. The reflectivity spectra presented in Fig. 9 reveal the materials' ability to reflect electromagnetic radiation at specific energy levels, which has significant technological implications, particularly in optoelectronic and photovoltaic applications. The high reflectivity values — reaching up to 69% for $NaAlTe_2$, 54% for $NaGaTe_2$, and 68% for $NaInTe_2$ along the [100] crystallographic direction, and similarly high values along the [001] direction — indicate strong interaction with incident photons at the corresponding energy levels (in the UV range). This behavior suggests that these materials can be effectively used in designing optical coatings, UV mirrors, and photodetectors. Furthermore, in the context of solar energy, understanding reflectivity is essential for optimizing light absorption and minimizing energy losses through reflection, thereby improving the efficiency of photovoltaic devices. The anisotropy observed between the [100] and [001] directions also provides insights into the directional dependence of optical performance, which is valuable for the development of advanced, orientation-dependent optoelectronic systems.

3.4.5. Loss function

The energy loss function of electrons, $L(\omega)$, is an important quantity that describes the energy loss of electrons passing through a material. When $\varepsilon_1(\omega) < 1$ and $\varepsilon_2(\omega)$ is close to 0, a frequency called the plasma frequency appears, at which the main peak in $L(\omega)$ is typically observed. The data presented in Fig. 10, illustrating the energy loss function $L(\omega)$ for $NaXTe_2$ compounds (X = Al, Ga, In), provide valuable insights into the technological potential of these compounds, particularly in plasmonic and optoelectronic applications. The peaks of $L(\omega)$ occur at the plasma energies, at which collective oscillations of conduction electrons take place, and indicate the ability of the materials to interact with high-energy photons. For $NaAlTe_2$, $NaGaTe_2$, and $NaInTe_2$, the plasma frequencies range from 4.65 to 16.41 in the [100] direction and from 4.84 to 15.55 in the [001] direction, with corresponding energy losses occurring in the ultraviolet region (approximately 14–16 eV).

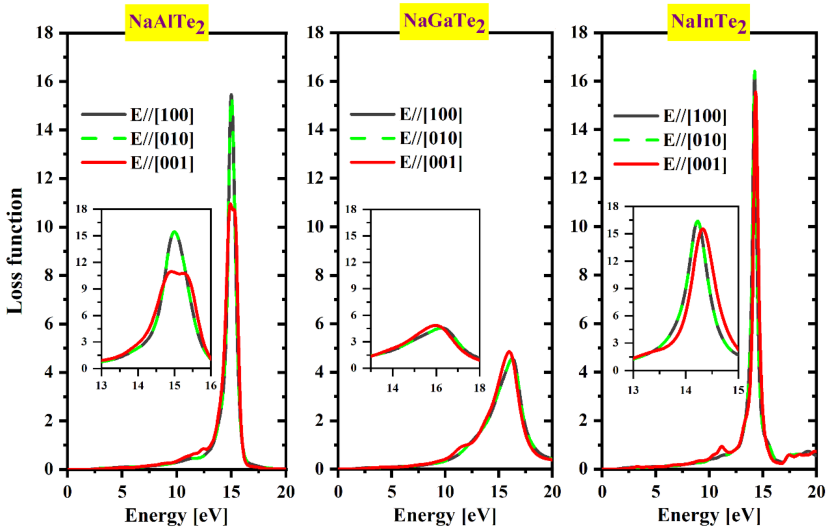

Fig. 10. Energy loss spectra of ternary chalcogenide compounds $NaXTe_2$ (X = Al, Ga, In).

These high plasma frequency values suggest that these compounds exhibit strong screening effects and significant electron density, making them promising candidates for applications involving UV shielding, energy filtering, or transparent conductive coatings. Furthermore, materials with such plasmonic properties can be utilized in advanced photonic devices, as sensors, solar cells, and high-frequency modulators. The directional dependence of the energy loss function also highlights anisotropic optical behavior, which can be exploited in the design of polarization-sensitive or directionally tunable optoelectronic components.

4. Conclusions

In this study, the structural, electronic, elastic, and optical properties of the ternary $NaXTe_2$ (X = Al, Ga, In) compounds were investigated using first-principles calculations based on density functional theory (DFT). Our findings confirm that these materials crystallize in a tetragonal structure within the $I_{4/mcm}$ space group, with optimized lattice parameters showing strong agreement with available experimental data. Electronic structure analysis indicates that $NaXTe_2$ compounds exhibit direct band gaps at the Z point, with values of 1.28 eV ($NaAlTe_2$), 0.23 eV ($NaGaTe_2$), and 0.58 eV ($NaInTe_2$), suggesting their potential use in optoelectronic applications. The density of states (DOS) analysis reveals strong hybridization between the X and Te atoms, confirming the covalent nature of the bonding.

The computed elastic properties of $NaXTe_2$ compounds, depending on the X atom, include the bulk modulus (ranging from 25.34 to 36.44 GPa), Young's modulus (from 30 to 75 GPa), Poisson's ratio (from 0.14 to 0.15), and anisotropy index (from 0.74 to 1.56). The results confirm the mechanical stability of the materials and classify them as soft, ductile materials with moderate hardness and anisotropic character. Besides that, compression is more difficult along the c axis, with B ranges from 100 to 140 GPa, compared to the a and b axis, where B lies between 68 and 100 GPa. Additionally, optical analysis reveals high absorption in the ultraviolet (UV) range, making these compounds suitable for optoelectronic and photovoltaic applications. Overall, our results provide valuable insights into the fundamental properties of $NaXTe_2$ compounds, highlighting their promising applications in semiconductor and optical technologies. Future work may focus on experimental validation and further exploration of their thermoelectric and electronic transport properties.

Acknowledgments

The authors thank Professor A. El Hdiy (ITheMM/EA7548), Université de Reims Champagne-Ardenne, Reims, France, and Professor M. Sidoumou, Université de Blida, for valuable discussions.

References

[1] M.H. Mia, F. Parvin, A.K.M.A. Islam, M.A. Khatun, *Int. J. Mod. Phys. B* **39**, 2550118 (2024).

[2] W.-H. Liu, W. Zeng, F.-S. Liu, B. Tang, Q.-J. Liu, X.-J. Ma, *J. Solid State Chem.* **303**, 122516 (2021).

[3] G. Behera, S.S. Nair, N. Singh, K.R. Balasubramaniam, A. Alam, *Phys. Rev. Appl.* **22**, 024042 (2024).

[4] A. Benmakhlouf, A. Bentabet, A. Bouhemadou, S. Maabed, R. Khenata, S. Bin-Omran, *Solid State Sci.* **48**, 72 (2015).

[5] T. Helaimia, A. Benmakhlouf, M. Bouchenafa, I. Messahli, S. Maabed, F. Khamloul, M. Sidoumoub, A. Bouhemadou, *Philos. Mag.* **102**, 69 (2022).

[6] M.S. Yaseen, G. Murtaza, R.M. Arif Khalil, *Opt. Quant. Electron.* **51**, 367 (2019).

[7] I.S. Khare, N.J. Szymanski, D. Gall, R.E. Irving, *Comput. Mater. Sci.* **183**, 109818 (2020).

[8] P. Koziarskyi, E.V. Maistruk, D.P. Koziarskyi, *Acta Phys. Pol. A* **142**, 607 (2022).

[9] P. Levinský, J. Hejtmánek, K. Knížek, M. Pashchenko, J. Navrátil, P. Masschelein, E. Dutková, P. Baláž, *Acta Phys. Pol. A* **137**, 904 (2020).

[10] S.S. Fouad, S.B. Youssef, *Acta Phys. Pol. A* **82**, 495 (1992).

[11] S. Sharma, A.S. Verma, V.K. Jindal, *Mater. Res. Bull.* **53**, 218 (2014).

[12] S. Tomar, R. Gautam, C.M.S. Negi, S.K. Gupta, S.R. Bhardwaj, A.S. Verma, *Chalcogenide Lett.* **16**, 1 (2019).

[13] H. Djamila, H. Belkhir, S. Ali, M. Bououdina, *Mater. Today Commun.* **37**, 107426 (2023).

[14] M.S. Yaseen, J. Sun, H. Fang, G. Murtaza, D.S. Sholl, *Solid State Sci.* **111**, 106508 (2021).

[15] Y. Harada, H. Nakanishi, S.F. Chichibu, *J. Appl. Phys.* **89**, 5406 (2001).

[16] V. Vorlíček, V. Železný, A.N. Tiwari, M. Krejci, H. Zogg, *J. Appl. Phys.* **82**, 5484 (1997).

[17] A.H. Reshak, M.G. Brik, S. Auluck, *J. Appl. Phys.* **116**, 103501 (2014).

[18] V. Jayalakshmi, S. Mageswari, B. Palanivel, *Solid State Phys.* **1447**, 1087 (2012).

[19] A.H. Reshak, S. Auluck, *Solid State Commun.* **145**, 571 (2008).

[20] V. Jayalakshmi, S. Davapriya, R. Murugan, B. Palanivel, *J. Phys. Chem. Solids* **67**, 669 (2006).

[21] M. Zhong, Z. Liu, Q.J. Liu, *Phys. Chem. Chem. Phys.* **27**, 7584 (2025).

[22] A.A. Lavrentyev, B.V. Gabrelian, V.T. Vu, L.N. Ananchenko, L.I. Isaenko, A.P. Yelisseyev, O.Y. Khyzhun, *Opt. Mater.* **66**, 149 (2017).

[23] B. Lagoun, T. Bentria, B. Bentria, *Comput. Mater. Sci.* **68**, 379 (2013).

[24] V.S. Khorkin, M.G. Milkov, S.N. Mantsevich, M.I. Kupreychik, S.I. Lobanov, V.N. Vedenyapin, *Opt. Mater.* **157**, 116202 (2024).

[25] Y.M. Basalaev, E.B. Duginova, E.V. Duginov, O.G. Basalaeva, *Solid State Commun.* **403**, 116005 (2025).

[26] W. Kohn, L.J. Sham, *Phys. Rev.* **140**, A1133 (1965).

[27] M.D. Segall, P.J.D. Lindan, M.J. Probert, C.J. Pickard, P.J. Hasnip, S.J. Clark, M.C. Payne, *J. Phys. Condens. Matter* **14**, 2717 (2002).

[28] J.P Perdew, K. Burke, M. Ernzerhof, *Phys. Rev. Lett.* **77**, 3865 (1996).

[29] D. Vanderbilt, *Phys. Rev B* **41**, 7892 (1990).

[30] J. Heyd, G.E. Scuseria, M. Ernzerhof, *J. Chem. Phys.* **118**, 8207 (2003).

[31] P.E. Blöchl, O. Jepsen, O.K. Andersen, *Phys. Rev. B* **49**, 16223 (1994).

[32] M.S. Yaseen, G. Murtaza, G. Murtaza, *Int. J. Mod. Phys. B* **34**, 2050133 (2020).

[33] K. Momma, F. Izumi, *J. Appl. Crystallogr.* **41**, 653 (2008).

[34] K. Choudhary, F. Tavazza, *Comput. Mater. Sci.* **161**, 300 (2019).

[35] K. Choudhary, I. Kalish, R. Beams, F. Tavazza, *Sci. Rep.* **7**, 5179 (2017).

[36] E.R. Franke, H. Schäfer, *Z. Naturforsch. B* **27**, 1308 (1972).

[37] K.P. Huber, G. Herzberg, *Molecular Spectra and Molecular Structure. IV. Constants of Diatomic Molecules*, Van Nostrand Reinhold, 1979.

[38] K.K. Irikura, *J. Phys. Chem. Ref. Data* **36**, 389 (2007).

[39] V.B. Lazarev, Z. Kish, Y. Peresh, E.E. Semrad, *Complex Chalcogenides in the AI–BIII–CVI Systems*, Metallurgiya, Moscow 1993.

[40] S. Haireche, M. Bouchenafa, M.A. Fadla, A. Benmakhlouf, S. Maabed, M. Sidoumou, *Acta Phys. Pol. A* **142**, 216 (2022).

[41] A. Kermezli, S. Haireche, M. Hassane, M. Bouchenafa, M. Elbaa, *J. Korean Phys. Soc.* **84**, 941 (2024).

[42] S. Haireche, A. Benmakhlouf, M. Bouchenafa, S. Maabed, M. Bouhamida, M. Sidoumou, *Sigma J. Eng. Nat. Sci.* **41**, 1231 (2023).

[43] B.O. Mnisi, *Eur. Phys. J. B* **98**, 42 (2025).

[44] F. Mouhat, F.-X. Coudert, *Phys. Rev. B* **90**, 224104 (2014).

[45] J. Wang, J. Li, S. Yip, S. Phillpot, D. Wolf, *Phys. Rev. B* **52**, 12627 (1995).

[46] A.P. Boresi, R.J. Schmidt, O.M. Sidebottom, *Advanced Mechanics of Materials* John Wiley & Sons, 1993.

[47] S.X. Tao, A.M.M.G. Theulings, V. Prodanović, J. Smedley, H. Van der Graaf, *Computation* **3**, 657 (2015).

[48] J. Friedel, C. Boulanger, C. Crussard, *Acta Metall.* **3**, 380 (1955).

[49] M. Bouchenafa, M. Sidoumou, M. Halit, A. Benmakhlouf, A. Bouhemadou, S. Maabed, A. Bentabet, S. Bin-Omran, *Solid State Sci.* **76**, 74 (2018).

[50] D.H. Chung, W.R. Buessem, *J. Appl. Phys.* **38**, 2535 (1967).

[51] J. Haines, J. Leger, G. Bocquillon, *Ann. Rev. Mater. Res.* **31**, 1 (2001).

[52] Z.-J. Wu, E.-J. Zhao, H.-P. Xiang, X.-F. Hao, X.-J. Liu, *J. Meng, Phys. Rev. B* **76**, 054115 (2007).

[53] V. Kanchana, G. Vaitheeswaran, Y. Ma, Y. Xie, A. Svane, O. Eriksson, *Phys. Rev. B* **80**, 125108 (2009).

[54] S.F. Pugh, *Lond. Edinb. Dubl. Philos. Mag. J. Sci.* **45**, 823 (1954).

[55] S.I. Ranganathan, M. Ostoja-Starzewski, *Phys. Rev. Lett.* **101**, 055504 (2008).

[56] A. Schleife, C. Rödl, J. Furthmüller, F. Bechstedt, *New J. Phys.* **13**, 085012 (2011).

[57] R.K. Giri, S.H. Chaki, M.S. Dave, S.R. Bharucha, A.J. Khimani, R.M. Kannaujiya, M.P. Deshpandea, M.B. Solankie, *Mater. Adv.* **4**, 3246 (2023).

[58] A. Kossa, M.T. Valentine, R.M. McMeeking, *Meccanica* **58**, 217 (2023).

[59] H. Zhang, C. Yuan, G. Yang, L. Wu, C. Peng, W. Ye, Y. Shen, H. Moayedi, *Eng. Comput.* **37**, 779 (2021).

[60] F. Molaei, *J. Geophys. Res. Solid Earth* **127**, e2021JB023681 (2022).

[61] V.J. Challis, X. Xu, A. Halfpenny, A.D. Cramer, M. Saunders, A.P. Roberts, T.B. Sercombe, *Acta Mater.* **254**, 119021 (2023).

[62] S. Eisebitt, T. Böske, J.-E. Rubensson, W. Eberhardt, *Phys. Rev. B* **47**, 14103 (1993).

[63] K. Meliani, S. Haireche, M. Bouchenafa, M. Elbaa, S. Douakh, R. Chiker, *Braz. J. Phys.* **54**, 46 (2024).

[64] S. Haireche, S. Douakh, M. Elbaa, M. Bouchenafa, K. Meliani, *Phys. B Condens. Matter* **696**, 416610 (2025).